Achieving Ultrahigh Power Factor In n-type Ag_2Se Thin Films by Carrier Engineering

Zhuang-Hao Zheng[1], Dong-Liang Zhang[1], Jun-Yu Niu[1], Xiao-Lei Shi[2,3], Tian-Bao Chen[1], Yun-Fei Chen[4], Fu Li[1], Guang-Xing Liang[1], Yue-Xing Chen[1,*], Ping Fan[1], Zhi-Gang Chen[2,*]

[1]Shenzhen Key Laboratory of Advanced Thin Films and Applications, Key Laboratory of Optoelectronic Devices and Systems of Ministry of Education and Guangdong Province, College of Physics and Optoelectronic Engineering, Shenzhen University, Shenzhen 518060, P. R. China.

[2]Centre for Future Materials, University of Southern Queensland, Springfield Central, Brisbane, Queensland 4300, Australia

[3]School of Chemistry and Physics, Queensland University of Technology, Brisbane City QLD 4000, Australia

[4]Hangzhou Innovation Institute, Beihang University, Hangzhou, 310052, P. R. China.

* Corresponding Author, Email: chenyx@szu.edu.cn; and zhigang.chen@uq.edu.au

Abstract

Ag_2Se-based thermoelectric materials are attracting great attention because of their potential in fabricating high-performance miniature and wearable electronics. Here, an advanced thermal co-evaporation method is employed to fabricate high-performance Ag_2Se thin films with controllable compositions. The atomic ratio Ag/Se of 2.06 can tune the carrier concentration to 1.4×10^{19} cm^{-3}, leading to a power factor of 6.27 μW cm^{-1} K^2 at room temperature. As well, an annealing process further improves the electrical transport properties by increasing the carrier mobility while maintaining the carrier concentration. Microstructure analysis indicates that annealing can reduce dislocation defect density and Ag vacancy concentration, contributing to a high Seebeck coefficient, finally resulting in a high power factor of 20.51 $\mu Wcm^{-1}K^{-2}$ at 393 K. Moreover, a thermoelectric device composed of 18 legs is fabricated by using the optimized Ag_2Se thin film, which presents a maximum output voltage and power of ~1.7 mV and ~22 nW at the temperature difference of 50 K. These results demonstrate that a combination of compositional optimization and annealing condition manipulation is effective to boost the thermoelectric performance of Ag_2Se thin films, showing great potentials in applying for wearable electronics.

Keywords: Ag_2Se; thin film; co-evaporation; annealing; power factor.

1. Introduction

Thermoelectric (TE) materials can utilize the Seebeck effect to produce electricity from thermal energy [1-5]. TE devices fabricated based on TE materials have wide applications in daily life, aerospace, military, and other fields due to the advantages of long service life and non-pollution [6-10]. The performance of TE materials is determined by the dimensionless figure-of-merit ZT ($ZT=S^2\sigma T/\kappa$), which is defined by the electrical conductivity σ, the Seebeck coefficient S, the thermal conductivity κ, and the absolute temperature T [11-14]. In terms of low dimensional TE materials, especially TE thin films, power factor ($PF = S^2\sigma$) is usually used to evaluate their TE performance.

Due to potential applications in miniature and wearable devices, achieving high-performance TE thin films is highly desired. Thin films fabricated based on traditional Te-based materials have been reported to exhibit high ZT values, but their high cost and poor mechanical properties still limit their applications [15]. As a promising n-type TE material, silver selenide (Ag_2Se) was reported to have a high ZT of 0.96 at 390 K [16]. Triggered by this, various methods have been employed to fabricate Ag_2Se thin films with the aim to achieve high TE performance and mechanical properties [17-22]. For example, Ag_2Se thin films, fabricated on the Nylon layer by hot-pressed, shows 9.87 μW cm^{-1} K^{-2} at room temperature [21] while Ag_2Se thin films, fabricated using the pulsed laser deposition method, shows a high PF of ~17.5 μW cm^{-1} K^{-2} at room temperature [20]. Besides, a high $S^2\sigma$ of 24.5 μW cm^{-1} K^{-2} at 303 K is achieved in the paper-supported Ag_2Se films, fabricated by a hydrothermal method [22].

Because both Ag and Se are easy to be oxidized, the vacuum physical vapor deposition technique is more suitable for preparing Ag_2Se thin films [17, 23-26]. A $S^2\sigma$ of 46.5 μW cm^{-1} K^{-2} at 376 K was reported in the stoichiometric Ag_2Se film, grown by pulsed hybrid reactive magnetron sputtering [17], which is comparable to that of the state-of-the-art bulk Ag_2Se [17]. The thermal evaporation method has been widely used to fabricate high-performance TE thin films, such as Bi_2Te_3 [27], Cu_2Se [28], and Sb_2Se_3 [29]. However, Ag_2Se thin films, prepared by the thermal evaporation method, have low $S^2\sigma$ [30-32] because of the serious deviation between the composition of the prepared film. Here, we use a facile

thermal co-evaporation method rather than using a single evaporated route to fabricate high-performance Ag_2Se thin films with controllable compositions. After the selective modification of Ag content [33-36], optimized n and σ are effectively realized. An annealing process is further employed to reduce the micro-structure defects of the films, leading to a significant enhancement of S. Accordingly, a high $S^2\sigma$ of 20.51 μW cm^{-1} K^{-2} is achieved at 393 K, which is a record-high value among the reported Ag_2Se thin films prepared by the co-evaporation methods.

2. Experimental details

Ag_2Se based thin films were deposited at room temperature by a thermal co-evaporation method. High purity Ag powder (99.99 %) and Se powder (99.99 %) were fixed in a vacuum deposition chamber by using tantalum evaporator boats. The BK7 glass was used as substrates with a dimension of 20 mm × 20 mm × 2 mm and ultrasonic-cleaned for 10 minutes sequentially in acetone, ethanol, and deionized water. The background pressure was maintained at 6.5 × 10^{-4} Pa. The working current of the silver source is 160 A, and the selenium source stabilized at 40 A with the deposition time was both 15 min. All the Ag and Se powders were evaporated after the deposition process. The weight ratio of Ag and Se powders was reasonably regulated in order to control the composition of thin films. The heat treatment of this work is carried out in the glove compartment under a nitrogen atmosphere, in which the content of water and oxygen is strictly controlled below 0.01 ppm. The heating table heats up at a speed of 1K/s, and the film sample is placed on the heating table for 30 minutes with a pressure of 30 KPa applied throughout the whole process, which is more conducive to uniform heating.

X-ray diffraction (XRD, D/max 2500 Rigaku Corporation, CuK_α radiation with the angle of 20° - 60° under a 0.02° per step) was applied to analyze the crystal orientation. The surface morphology and element distribution were characterized by scanning electron microscopy (SEM, Zeiss supra55) and transmission electron microscopy (TEM, Titan Cubed Themis G201, FEI) with an energy

dispersive spectrometer (EDS, Bruker EDS QUANTAX). The σ and S were measured by utilizing a Seebeck coefficient and electrical conductivity apparatus (SBA458, Nezsch). Van der Pauw Hall measuring instrument (HL5500 PC, Nanometrics) was applied to investigate the n and μ. The uncertainty of the Seebeck coefficient and electrical conductivity are 7 % and 5 %, respectively, and the uncertainty of carrier concentration and carrier mobility is about 10 %. X-ray photoelectron spectroscopy (XPS, Thermo escalab 250Xi Thermo Fisher) provided semi-quantitative information of the elemental valence states. Variable temperature XRD (SmartLab 3KW Rigaku Corporation) was used to determine the phase transition at 406 K. The bandgap was determined from the reflection spectra obtained on UV-VIS-NIR spectrometer (UV-3600Plus Shimadzu Corporation). The first-principles density functional calculations are implemented in the CASTEP code. A plane-wave cutoff energy of 300 eV based on the ultrasoft pseudopotentials to express the interaction between electrons and ions [34]. The Ag $4d^{10}5s^{1}$, Se $4s^{2}4p^{4}$ electrons are treated as valence states. The generalized gradient approximation of Perdew-Burke-Ernzerhof (GGA-PBE) is adopted for the exchange and correlation function:

$$E_{xc}^{GGA}[\rho]=\int f_{xc}\left(\rho(\boldsymbol{r}),|\nabla\rho(\boldsymbol{r})|\right)d\boldsymbol{r} \quad (1)$$

The Ag_2Se structure is relaxed until the forces on each atom are less than 0.03 $eVnm^{-1}$, and the criteria for energy convergence is set as 1.0×10^{-5} eV, A Monkhorst-Pack k-point mesh of 3×3×3 is adopted for sampling the Brillouin zone (BZ) of the Ag_2Se unit cell. The Ag vacancy Ag_2Se is constructed based on a 2×2×1 supercell of Ag_2Se. And we followed the geometrical optimization method BFGS. The stress in the crystal of 0.05 GPa, and the maximum displacement of atoms of 0.0001 nm.

3. Results and discussion

Fig. 1(a) illustrates our thermal co-evaporation method to deposit Ag_2Se thin films. **Table S1** in Supporting information summarizes the composition contents of Ag_2Se thin films, measured by EDS, indicating that the actual atomic ratios are close to the nominal values. According to the compositions,

the films are described by using actual atomic ratios as $Ag_{1.60}Se$, $Ag_{1.65}Se$, $Ag_{1.91}Se$, $Ag_{1.97}Se$, $Ag_{2.06}Se$, $Ag_{2.15}Se$, and $Ag_{2.33}Se$. **Fig.1(b)** shows the XRD patterns of thin films. As can be seen, three main peaks for all the patterns are located at ~33.5°, ~34.7°, and ~36.9°, corresponding to the (112), (121), and (013) planes of Ag_2Se polycrystalline (PDF#24-1041) [37]. The $Ag_{1.60}Se$ and $Ag_{1.65}Se$ contain weak impurity peaks at ~29.5°, belonging to the Se phase (PDF#06-0362), which disappears with increasing the Ag content. Meanwhile, all samples have Ag impurity peaks at ~38.1°. With increasing Ag content, this peak intensity increases, as indicated in **Fig. 1(b)** (right). Elemental mappings in **Fig. 2(c-e)** confirm Se clusters in the Se-rich samples [38], and no Se-rich parts can be observed when Ag increases, matching with the XRD results. However, some particles are observed on the surface of Ag-rich thin film and confirmed as Ag clusters [30], indicating that the thin film deposited at room temperature has some component defects, which are mainly due to the insufficient atomic energy as shown in the surface morphology (**Fig. S1** (Supporting information)).

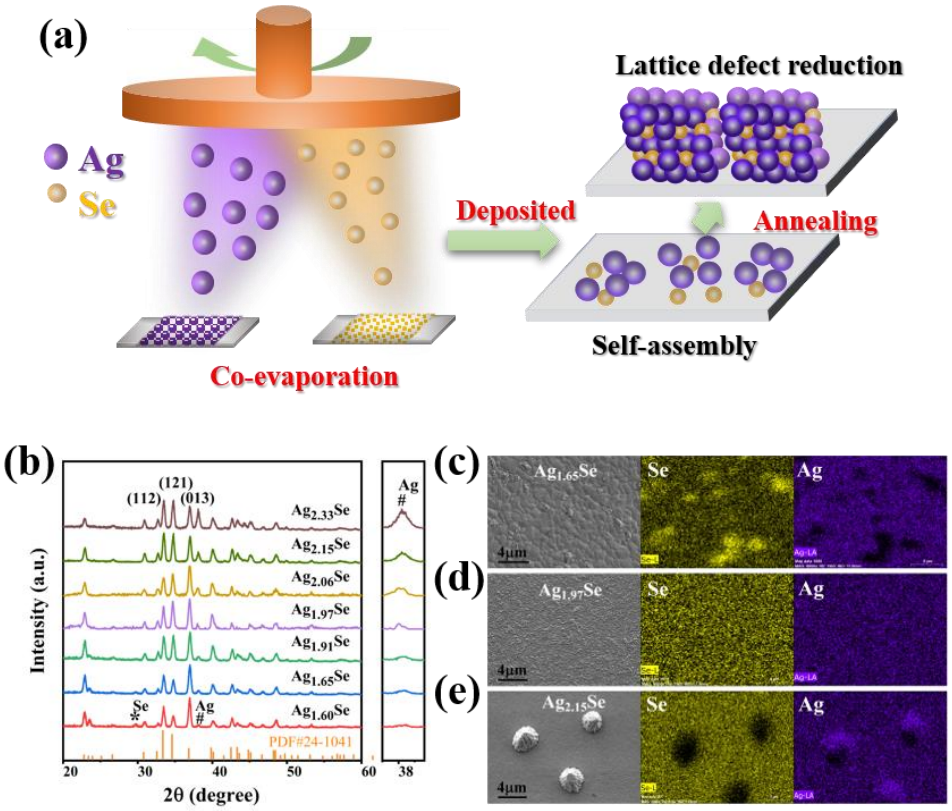

Fig.1 (a) Schematic of the thermal co-evaporated Ag_2Se based thin films. (b) X-ray diffraction (XRD)

patterns of Ag_2Se thin films with different atomic ratios of Ag to Se. (c)~(e) Surface morphology and elemental mappings of $Ag_{1.65}Se$, $Ag_{1.97}Se$, and $Ag_{2.15}Se$ thin films.

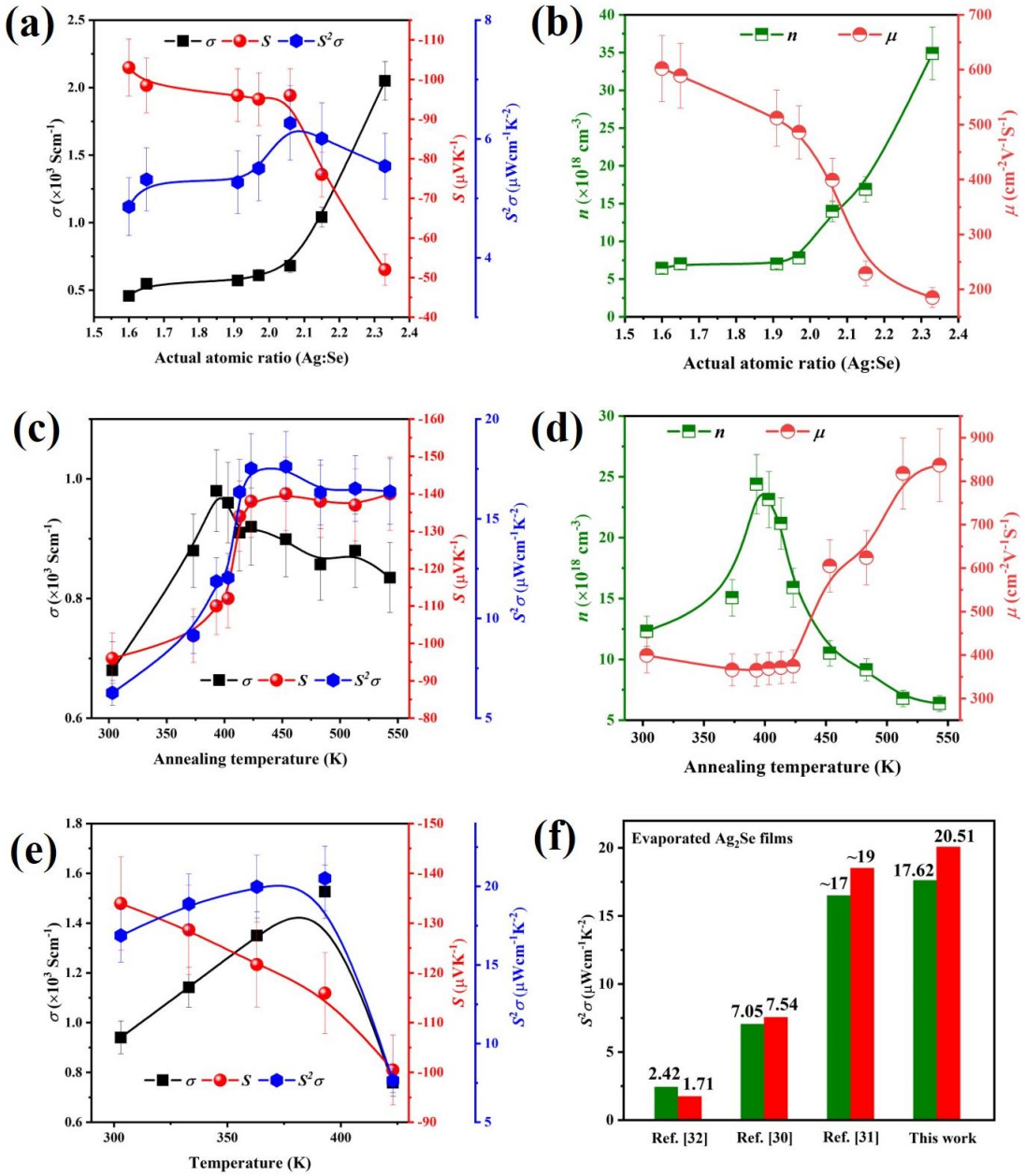

Fig.2 (a) Room-temperature electrical conductivity σ, Seebeck coefficient S, and power factor ($S^2\sigma$) of the thin films with various compositions; (b) Carrier concentration n and mobility μ of the Ag_2Se thin films with different atomic ratios of Ag to Se; (c) σ, S and $S^2\sigma$ as a function of annealing temperature for $Ag_{2.06}Se$ sample; (d) n and μ of the annealed samples; (e) Temperature-dependent σ, S, and $S^2\sigma$ of the thin films annealed at 423 K; (f) The comparison of $S^2\sigma$ (green for 300 K and red for 393 K) of

Ag_2Se thin films prepared by the thermal evaporation method [30-32].

Fig. 2(a) shows the room-temperature σ, S, and $S^2\sigma$ of the Ag_2Se-based thin films. With increasing the Ag content, the σ increases while the S decreases. As a result, $S^2\sigma$ is firstly increased, reaching a maximum value of 6.27 μW cm^{-1} K^{-2} at room temperature, and then decreased. According to the Mott equation [29], both σ and S are determined by n and μ:

$$\sigma = en\mu \tag{2}$$

$$S = \frac{8\pi^2 k_B^2 T m^*}{3eh^2}\left(\frac{\pi}{3n}\right)^{2/3} \tag{3}$$

where m^* is the effective mass of electrons, k_B is the Boltzmann constant, h is the Planck constant and e is the carrier charge. **Fig. 2(b)** displays the n and μ as a function of the Ag to Se atomic ratio. The n of the $Ag_{1.6}Se$ is 6.4×10^{18} cm^{-3}, and then greatly increases to $> 1.4\times10^{19}$ cm^{-3} after the atomic ratio raised over 2.06, while the μ corresponding decreases from 602 cm^{-2} V^{-1} s^{-1} to 399 cm^{-2} V^{-1} s^{-1}. It can be noted that the change of n is more distinct than that of the μ due to the disappeared Se defect and the increased Ag content, thus attributing to the greatly enhanced σ [40].

Although thin films deposited at room-temperature have high n values, some Ag clusters can be observed from the SEM results, leading to low μ and in turn the low $S^2\sigma$ [33]. Annealing was reported as an efficient way to reduce the defects and increase the grain size of the thin films, leading to high μ [22]. On this basis, the $Ag_{2.06}Se$ sample with a maximum $S^2\sigma$ value was performed *via* an annealing process and the annealing temperatures were set as 375 K, 393 K, 403 K, 413 K, 423 K, 453 K, 483 K, 513 K, and 543 K. **Fig. 2(c)** shows the σ, S, and $S^2\sigma$ as a function of annealing temperature. Both σ and S are increased after annealing, and all the annealed thin films have higher σ and S values than that of the as-deposited samples. A maximum $S^2\sigma$ value of 17.62 μW $cm^{-1}K^{-2}$ can be obtained for the sample annealed at 423 K, which is over 200 % enhancement compared with the as-deposited sample. **Fig. 2(d)** shows the n and μ as a function of annealing temperature. With increasing the annealing

temperature, the *n* is firstly increased and then decreased, which is well-matched with the change of σ. **Table S2** in Supporting information shows EDS results of $Ag_{2.06}Se$ films annealed at different temperatures, indicating that the Se content is slightly decreased after annealing, resulting in the decreased *n*. Especially, μ is greatly increased to over 600 cm^{-2} V^{-1} s^{-1} with the slight effect in the *n* when the annealing temperature was over 393 K, benefiting to achieve high *S* and $S^2\sigma$. Additionally, the temperature-dependent TE performance of the sample annealed at 423 K is shown in **Fig. 2(e)**, indicating an increasing trend with the increasing test temperature. The σ of 1526.5 S cm^{-1} and *S* of 115.9 μV K^{-1} are obtained at 393 K, contributing to a maximum $S^2\sigma$ of 20.51 μW cm^{-1} K^{-2}. The achieved $S^2\sigma$ values at room temperature and 393 K are the record-high values for the Ag_2Se based thin films prepared by the thermal evaporation method, as shown in **Fig. 2(f)**, and be comparable to other n-type thermoelectric thin films, such as Yb-filled $CoSb_3$, TiS_2, Bi_2Te_3, *et al.,* as shown in **Table 1** [41-46].

Table 1 Thermoelectric properties, including electrical conductivity (σ), Seebeck coefficient (*S*), and maximum power factor PF_{max} at the optimum temperature of the present Ag_2Se thin films and other reported n-type thin films.

Samples	**σ (S cm^{-1})**	**S (μV K^{-1})**	**$S^2\sigma$ (μW cm^{-1} K^{-2})**	***Ref***
$Ag_{2.06}Se$	899	-140	17.62	**This work**
Yb-filled $CoSb_3$	110	-260	7.4	[41]
$SrTi_{0.8}Nb_{0.2}O_3$	~325	~-200	~13.0	[42]
HgSe	20	-518	5.5	[43]
Ag_2Te	95.3	-142	1.92	[44]
TiS_2	790	-75.5	9.04	[45]
Bi_2Te_3	~600	~-140	~11.8	[46]

In order to understand our high performance after annealing, we further characterized the annealed thin films. **Fig.3(a)** shows the XRD patterns of the annealed thin films. All the thin films show the primary Ag_2Se phase with a weak impurity Ag. With increasing the annealing temperature,

the intensity of (112) peak increases and (121) peak decreases, which is more closed to the typical α-phase Ag_2Se. The binding states of Ag and Se elements in the $Ag_{2.06}Se$ thin film were investigated by XPS, and the results are illustrated in **Fig. 3(b-c)**. As shown in **Fig. 3(b)**, the core level spectrums reveal that the sample has two strong peaks located at ~368.4 eV of Ag $3d_{5/2}$ and ~374.2 eV of Ag $3d_{3/2}$, which agree with the spin-orbit phenomena of Ag and Ag^+, respectively [40]. A broad peak ranging from 52 to 56 eV is observed, and can be identified into two symmetric peaks to be assigned to Se $3d_{5/2}$ and Se $3d_{3/2}$ located at ~54.2 and ~54.9 eV, which is the characteristic shape of Se(−II) in a consistent bonding environment, as shown in **Fig. 3(c)** [40]. These analyses indicate that the chemical states of the elements of the thin films are Ag^+ and Se^{2-}. SEM images of the annealed thin films are shown in **Fig. S2**, indicating that the surfaces of all the thin films have Ag clusters. However, more Ag spherical-liked clusters are observed when the annealing temperature is over 483 K. These independent Ag clusters in the thin film surface (**Fig. S3**) act as a combining center, leading to the decrease σ [30]. The content of Se is slightly decreased after annealing, as shown in EDS results (**Table S2**), suggesting that the aggravation of element diffusion during the annealing process, which leads to the strength of Ag clusters and the loss of Se. These results are consistent with the previous literature [30,32].

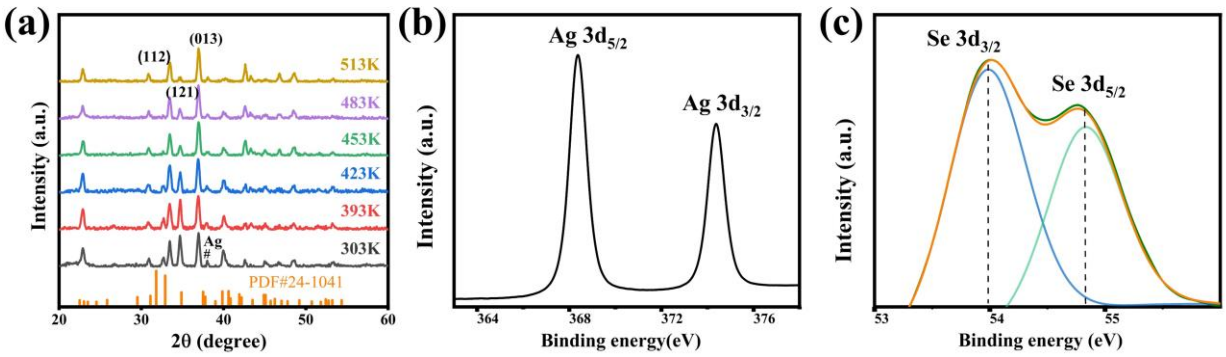

Fig. 3 (a) XRD patterns of Ag_2Se based thin films with different annealing temperatures. X-ray photoelectron spectroscopy (XPS) survey scans of $Ag_{2.06}Se$ thin film for (b) Ag and (c) Se.

It is worth noting that the annealing temperature corresponding to the sharp increase in the μ is

near the phase-transition temperature from α-phase to β-phase of Ag_2Se (*in-situ* XRD shown in **Fig. S4**). Thus, in order to further investigate the factor, the unannealed $Ag_{2.06}Se$ sample and annealed sample at 423 K were analyzed by TEM. As shown in **Fig.4 (a)**, screw dislocations with lengths of ~100 nm are observed for unannealed thin film. Moreover, Ag vacancies in the lattice are observed in **Fig. 4(a)**, which are further confirmed by the intensity line profile of the square root of scanning transmission electron microscope (STEM) intensity. It can be speculated that there is still a lack of Ag in some regions due to the Ag-clusters, despite the thin film being slight Ag-rich. As mentioned above in the SEM analysis that some independent Ag clusters are distributed in the surface of the thin film due to the limit of diffusion energy of the atoms when the thin film was deposited at room temperature. For annealed $Ag_{2.06}Se$ film, no dislocations are observed in the measurement region, and Ag vacancy is also disappeared from the grains, indicating the redistribution of atoms during the annealing process. The reduction of defects is beneficial to the transport of carriers, and the vanishment of Ag vacancies induces the decrease of n. These analyses are consistent with the transport properties as displayed in **Fig. 3**. We also employed DFT calculations to investigate the variations in band structures of Ag_2Se with and without Ag vacancies. The calculation results in **Fig. 4(c)** and **Fig. 4(d)** show that the Ag_2Se with Ag vacancies has a smaller bandgap than that of the pure Ag_2Se. In **Fig. S5**, the measured optical bandgap confirms that the films have a larger optical bandgap after annealing, which matches the calculated results. Additionally, more Ag atoms can enter the β-phase lattice than the α-phase as reported in the literature [35,36]. Therefore, it can be inferred that the intensified atomic diffusion at the annealing temperature over phase change temperature can reduce dislocation defects and Ag vacancy defects in the Ag_2Se thin film, thus contributing to the enhancement of μ and resulting in relative high S.

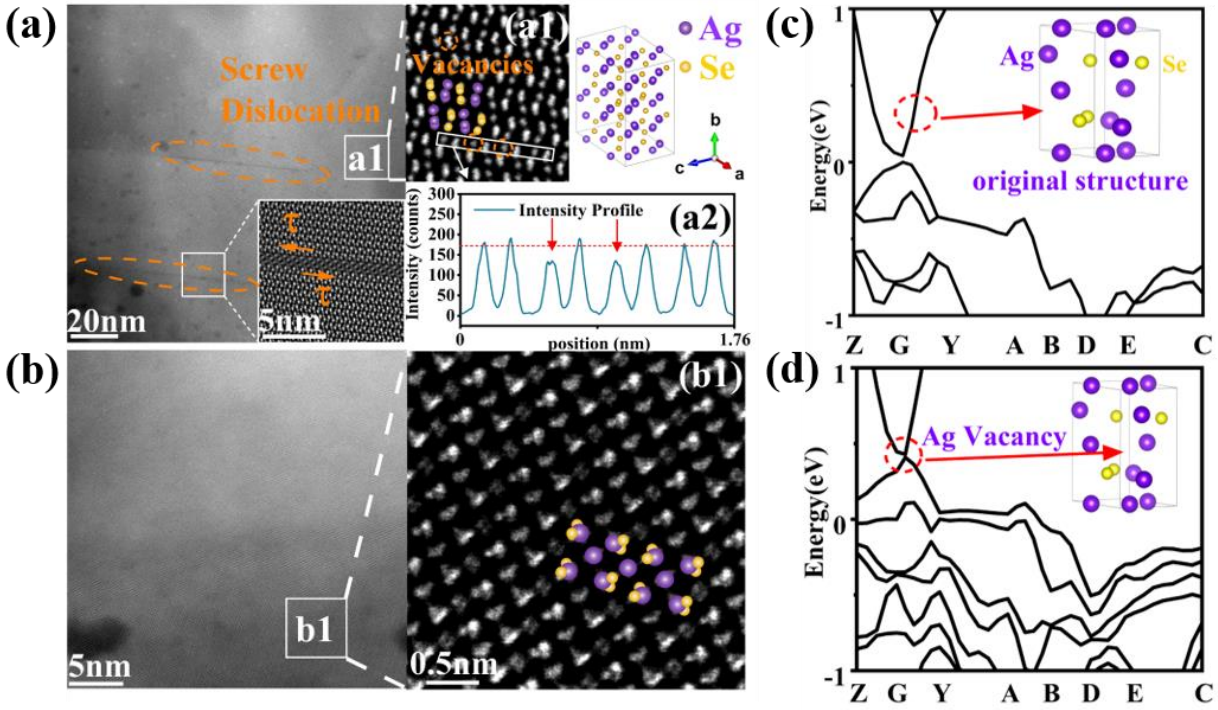

Fig. 4 (a) Transmission electron microscope (TEM) images of the $Ag_{2.06}Se$ film before heat treatment, screw dislocation, and Ag vacancies (a1) are observed in the lattices; (a2) Intensity line profile of the square root of scanning transmission electron microscope (STEM) intensity. (b) Low magnification TEM and high-resolution TEM images of the $Ag_{2.06}Se$ after annealing at 423 K. (c) Band structure and lattice structure of primary phase of silver selenide. (d) Band structure and lattice structure of silver selenide contain vacancy defects.

Using the n-type Ag_2Se based films, we also prepared a TE power generator composed of 18 legs and connected by using Cu electrode as shown in **Fig.S6** (optical photo, Supporting Information). **Fig. 5(a)** presents the output voltage and the output power of the TE device as a function of current at different temperature differences ΔTs. The voltage increases monotonically as ΔT increases from 30 °C to 50 °C, where it reaches the maximum of ~1.7 mV. The maximum P_{max} can be obtained at the condition of R_{ex} (external resistance) = R_{in} (internal resistance). P_{max} values are ~12 nW, ~16 nW, and ~22 nW when the ΔTs are 30 °C, 40 °C, and 50 °C, respectively. Additionally, by creating a temperature

difference by laser, the output voltage can reach 0.3 mV (**Fig.5(b)**), clearly showing the possibility of direct conversion of light into electricity.

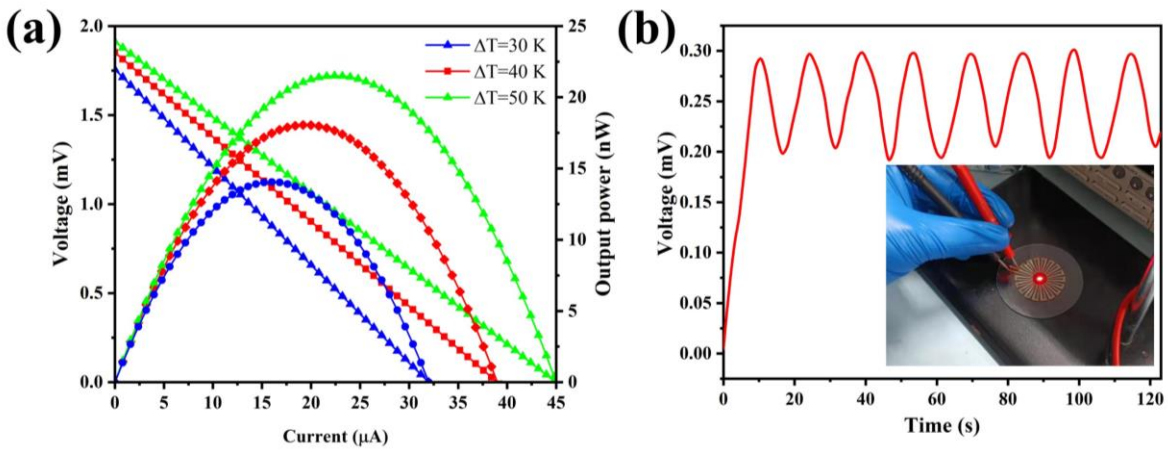

Fig. 5 (a) Output voltage and power as a function of current under different temperature differences. (b) Output voltage of the TE device under laser irradiation.

4. Conclusion

In summary, high-performance Ag_2Se thin films are fabricated at room temperature by using a thermal co-evaporation method. After carrier concentration optimization by controlling Ag content, σ increases and results in a maximum $S^2\sigma$ of 6.27 $\mu Wcm^{-1}K^{-2}$. Subsequently, the S of the prepared thin films is greatly enhanced after employing an annealing process due to the reduced dislocation defects and Ag vacancies. As a result, an ultrahigh $S^2\sigma$ of 17.62 $\mu W\ cm^{-1}\ K^2$ at room temperature and 20.51 $\mu W\ cm^{-1}\ K^2$ at 393 K are obtained. A thin-film thermoelectric device fabricated by using this n-type Ag_2Se indicates the stable output voltage and power at different temperature differences. Besides, the device can generate a stable output voltage of ~0.3 mV under intermittent laser irradiation. The overall performance of thermoelectric properties in this work is comparable or even higher than that of previously reported Ag_2Se thin films prepared by the thermal evaporation method.

Acknowledgments

This work was supported by the National Natural Science Foundation of China (Grant No. 11604212), Guangdong Basic and Applied Basic Research Foundation (2020A1515010515 and

2019A1515110107), and Science and Technology plan project of Shenzhen (20200811230408001). The authors are thankful for the assistance on STEM-HAADF observation received from the Electron Microscope Center of the Shenzhen University.

References

[1] G. Tan, L.D. Zhao, M.G. Kanatzidis, Rationally designing high-performance bulk thermoelectric materials, Chem. Rev., 116 (2016) 12123-12149.

[2] P. Fan, X.L. Huang, T.B. Chen, F. Li, Y.B. Chen, B. Jabar, S. Chen, H.L. Ma, G.X. Liang, J.T. Luo, X.H. Zhang, Z.H. Zheng, α-Cu_2Se thermoelectric thin films prepared by copper sputtering into selenium precursor layers, Chem. Eng. J., 410 (2021) 128444.

[3] Z.H. Zheng, T. Wang, D. Yang, B. Jabar, A. Abbas, F. Li, Y.X. Chen, X.H. Zha, G.X. Liang, P. Fan. Nanostructural Manipulations for Achieving Record-High Room Temperature Figure of Merit in the Znsb Thin Films, Mater. Today Energy, 22 (2021) 100870.

[4] L. Hu, H. Wu, T. Zhu, C. Fu, J. He, P. Ying, X. Zhao, Tuning multiscale microstructures to enhance thermoelectric performance of n-type bismuth-telluride-based solid solutions, Adv. Energy Mater., 5 (2015) 1500411.

[5] Z. H. Zheng, X. L. Shi, D. W. Ao, W.D. Liu, Y. X. Chen, F. Li, S. Chen, X. Q. Tian, X. R. Li, J. Y. Duan, H. L. Ma, X. H. Zhang, G. X. Liang, P. Fan, Z. G. Chen, Rational band engineering and structural manipulations inducing high thermoelectric performance in n-type $CoSb_3$ thin films, Nano Energy, 81 (2021) 105683.

[6] K. Buks, J. Andzane, K. Smits, J. Zicans, J. Bitenieks, A. Zarins, D. Erts, Growth mechanisms and related thermoelectric properties of innovative hybrid networks fabricated by direct deposition of Bi_2Se_3 and Sb_2Te_3 on multiwalled carbon nanotubes, Mater. Today Energy, 18 (2020) 100526.

[7] L. X. Huang, D.W. Ao, T. B. Chen, Y. X. Chen, F. Li, S. Chen, G. X. Liang, X. H. Zhang, Z. H.

Zheng, P. Fan, High-performance copper selenide thermoelectric thin films for flexible thermoelectric application, Mater. Today Energy, 21(2021) 100743.

[8] R. Nunna, P. Qiu, M. Yin, H. Chen, R. Hanus, Q. Song, T. Zhang, M.-Y. Chou, M.T. Agne, J. He, G.J. Snyder, X. Shi, L. Chen, Ultrahigh thermoelectric performance in Cu_2Se-based hybrid materials with highly dispersed molecular CNTs, Energ. Environ. Sci., 10 (2017) 1928-1935.

[9] A.A. Olvera, N.A. Moroz, P. Sahoo, P. Ren, T.P. Bailey, A.A. Page, C. Uher, P.F.P. Poudeu, Partial indium solubility induces chemical stability and colossal thermoelectric figure of merit in Cu_2Se, Energ. Environ. Sci., 10 (2017) 1668-1676.

[10] X.L. Shi, J. Zou, Z.G. Chen, Advanced thermoelectric design: from materials and structures to devices, Chem. Rev. 120 (2020) 7399-7515.

[11] S.D. Xu, M. Hong, M. Li, Q. Sun, Y. Yin, W.D. Liu, X.L. Shi, M. Dargusch, J. Zou, Z. G. Chen, Two-dimensional flexible thermoelectric devices: Using modeling to deliver optimal capability, Appl. Phys. Rev. 8 (2021) 041404.

[12] C. Jiang, P. Wei, Y. Ding, K. Cai, L. Tong, Q. Gao, Y. Lu, W. Zhao, S. Chen, Ultrahigh performance polyvinylpyrrolidone/Ag_2Se composite thermoelectric film for flexible energy harvesting, Nano Energy, 80 (2021) 105488.

[13] S.D. Xu, X.L. Shi, M. Dargusch, C. A. Di, J. Zou, Z.G. Chen, Conducting polymer-based flexible thermoelectric materials and devices: From mechanisms to applications, Prog. Mater. Sci., 121 (2021) 100840.

[14] L. Zhang, X.L. Shi, Y.L. Yang, Z.G. Chen, Flexible thermoelectric materials and devices: From materials to applications, Mater. Today, 46 (2021) 62-108.

[15] Y. Wang, W. D. Liu, X.-L. Shi, M. Hong, L. J. Wang, M. Li, H. Wang, J. Zou, Z. G. Chen,

Enhanced thermoelectric properties of nanostructured n-type Bi_2Te_3 by suppressing Te vacancy through non-equilibrium fast reaction, Chem. Eng. J., 391 (2020) 123513.

[16] H. Z. Duan, Y. L. Li, K. P. Zhao, P. F. Qiu, X. Shi, L. D. Chen, Ultra-fast synthesis for Ag_2Se and CuAgSe thermoelectric materials, JOM, 68 (2016) 2659-2665.

[17] J.A. Perez-Taborda, O. Caballero-Calero, L. Vera-Londono, F. Briones, M. Martin-Gonzalez, High thermoelectric zT in n-type silver selenide films at room temperature, Adv. Energy Mater., 8 (2018) 1702024.

[18] Y. Lu, Y. Qiu, K. Cai, Y. Ding, M. Wang, C. Jiang, Q. Yao, C. Huang, L. Chen, J. He, Ultrahigh power factor and flexible silver selenide-based composite film for thermoelectric devices, Energ. Environ. Sci., 13 (2020) 1240-1249.

[19] C.H. Xin, Z.L. Hu, Z.Q. Fang, M. Chaudhary, H.Y. Xiang, X.Z. Xu, L. Aigouy, Z.Y. Chen, Flexible and wearable plasmonic-enabled organic/inorganic hybrid photothermoelectric generators, Mater. Today Energy, 22 (2021) 100859.

[20] K. Zhou, J. Chen, R. Zheng, X. Ke, T. Zhang, X. Shi, L. Chen, Non-epitaxial pulsed laser deposition of Ag_2Se thermoelectric thin films for near-room temperature applications, Ceram. Int., 42 (2016) 12490-12495.

[21] Y. Ding, Y. Qiu, K. Cai, Q. Yao, S. Chen, L. Chen, J. He, High performance n-type Ag_2Se film on nylon membrane for flexible thermoelectric power generator, Nat. Commun., 10 (2019) 841.

[22] J. Gao, L. Miao, H. Lai, S. Zhu, Y. Peng, X. Wang, K. Koumoto, H. Cai, Thermoelectric flexible silver selenide films: compositional and length optimization, iScience, 23 (2020) 100753.

[23] M. C. S. Kumar, B. Pradeep, Transport properties of silver selenide thin films from 100 to 300K, Mater. Lett., 56 (2002) 491-495.

[24] P. Gnanadurai, N. Soundararajan, C.E. Sooriamoorthi, Influence of heating rate on the hysteresis in the phase transition in silver selenide thin films, Vacuum, 78 (2005) 33-36.

[25] M. Pandiaraman, N. Soundararajan, C. Vijayan, C. Kumar, R. Ganesan, Spectroscopic studies on silver selenide thin films, J. Ovonic Res., 6 (2010) 285-295.

[26] S. Hussain, J. Chae, K. Akbar, D. Vikraman, L. Truong, B.A. Naqvi, Y. Abbas, H.S. Kim, S.H. Chun, G. Kim, J. Jung, Fabrication of robust hydrogen evolution reaction electrocatalyst using Ag_2Se by vacuum evaporation, Nanomaterials, 9 (2019) 1460.

[27] Z. Wu, J. Wu, Y. Li, G. Li, Effect of Cu content on electrical properties of evaporated Cu-Se thermoelectric films, Ceram. Int., 46 (2020) 21617-21622.

[28] R. Tang, Z. Wang, W. Li, L. Feng, J. Zhang, L. Wu, B. Li, G. Zeng, W. Wang, Bi_2Te_3 thin films prepared by co-evaporation for CdTe thin film solar cells, Sol. Energ. Mat. Sol. C, 121 (2014) 92-98.

[29] L. Zhang, Y. Li, C. Li, Q. Chen, Z. Zhen, X. Jiang, M. Zhong, F. Zhang, H. Zhu, Scalable low-band-gap Sb_2Se_3 thin-film photocathodes for efficient visible-near-infrared solar hydrogen evolution, ACS Nano, 11 (2017) 12753-12763.

[30] S. Jindal, S. Singh, G.S.S. Saini, S.K. Tripathi, Enhanced thermopower in (013)-oriented silver selenide films produced by thermal annealing, App. Phys. A, 126 (2020) 374.

[31] S. Hou, Y. Liu, L. Yin, C. Chen, Z. Wu, J. Wang, Y. Luo, W. Xue, X. Liu, Q. Zhang, F. Cao, High performance wearable thermoelectric generators using Ag_2Se films with large carrier mobility, Nano Energy, 87 (2021) 106223.

[32] S. Jindal, S. Singh, G.S.S. Saini, S.K. Tripathi, Low temperature thermoelectric power factors of thermally evaporated Ag_2Se thin films, AIP Conf. Proc., 2220 (2020) 090008.

[33] C. Lee, Y.-H. Park, H. Hashimoto, Effect of nonstoichiometry on the thermoelectric properties of

a Ag_2Se alloy prepared by a mechanical alloying process, J. Appl. Phys., 101 (2007) 024920.

[34] F. Yang, S. Xiong, Z. Xia, F. Liu, C. Han, D. Zhang, Two-step synthesis of silver selenide semiconductor with a linear magnetoresistance effect, Semicond. Sci. Tech., 27 (2012) 125017.

[35] B.C. Mohanty, S. Kasiviswanathan, Thermal stability of silver selenide thin films on silicon formed from the solid state reaction of Ag and Se films, Thin Solid Films, 515 (2006) 2059-2065.

[36] Y.S. Tveryanovich, A.A. Razumtcev, T.R. Fazletdinov, A.S. Tverjanovich, E.N. Borisov, Fabrication of stoichiometric oriented Ag_2Se thin film by laser ablation, Thin Solid Films, 666 (2018) 172-176.

[37] B. Mogwitz, C. Korte, J. Janek, M. V. Kreutzbruck, L. Kienle, Preparation and magnetoresistance of $Ag_{2+x}Se$ thin films deposited *via* pulsed laser deposition, J. Appl. Phys., 101 (2007) 043510.

[38] D. Milašienė, R. Ivanauskas, Silver selenide modification of polyamide fabric, Open Chem., 11 (2013) 1976-1980.

[39] M. von Kreutzbruck, B. Mogwitz, F. Gruhl, L. Kienle, C. Korte, J. Janek, Magnetoresistance in $Ag_{2+\delta}Se$ with high silver excess, Appl. Phys. Lett., 86 (2005) 072102.

[40] B.C. Mohanty, P. Malar, T. Osipowicz, B.S. Murty, S. Varma, S. Kasiviswanathan, Characterization of silver selenide thin films grown on Cr-covered Si substrates, Surf. Int. Anal., 41 (2009) 170-178.

[41] G. Fu, L. Zuo, J. Chen, M. Lu, L. Yu, Thermoelectric properties of DC-sputtered filled skutterudite thin film, J. Appl. Phys., 117 (2015) 125304.

[42] S. Ohta, T. Nomura, H. Ohta, M. Hirano, H. Hosono, K. Koumoto, Large thermoelectric performance of heavily Nb-doped $SrTiO_3$ epitaxial film at high temperature, Appl. Phys. Lett., 87 (2005) 092108.

[43] J. Choi, K. Cho, J. Yun, Y. Park, S. Yang, S. Kim, Large voltage generation of flexible thermoelectric nanocrystal thin films by finger contact, Adv. Energy Mater., 7 (2017) 1700972.

[44] J. Gao, L. Miao, C. Liu, X. Wang, Y. Peng, X. Wei, J. Zhou, Y. Chen, R. Hashimoto, T. Asaka, K. Koumoto, A novel glass-fiber-aided cold-press method for fabrication of n-type Ag_2Te nanowires thermoelectric film on flexible copy-paper substrate, J. Mater. Chem. A, 5 (2017) 24740-24748.

[45] C. Wan, X. Gu, F. Dang, T. Itoh, Y. Wang, H. Sasaki, M. Kondo, K. Koga, K. Yabuki, G.J. Snyder, R. Yang, K. Koumoto, Flexible n-type thermoelectric materials by organic intercalation of layered transition metal dichalcogenide TiS_2, Nat. Mater., 14 (2015) 622-627.

[46] T. Cao, X.L. Shi, J. Zou, Z.G. Chen, Advances in conducting polymer-based thermoelectric materials and devices, Microstructures 1 (2021) 1-33.